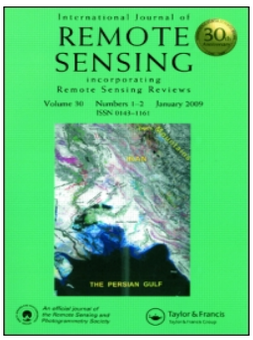

International Journal of Remote Sensing

ISSN: 0143-1161 (Print) 1366-5901 (Online) Journal homepage: http://www.tandfonline.com/loi/tres20

Horizontal advection of temperature and salinity by Rossby waves in the North Pacific

Tatyana V. Belonenko, Igor L. Bashmachnikov & Arseny A. Kubryakov

To cite this article: Tatyana V. Belonenko, Igor L. Bashmachnikov & Arseny A. Kubryakov (2018) Horizontal advection of temperature and salinity by Rossby waves in the North Pacific, International Journal of Remote Sensing, 39:8, 2177-2188, DOI: 10.1080/01431161.2017.1420932

To link to this article: https://doi.org/10.1080/01431161.2017.1420932

INTERNATIONAL JOURNAL OF REMOTE SENSING, 2018
VOL. 39, NO. 8, 2177–2188
https://doi.org/10.1080/01431161.2017.1420932

Taylor & Francis
Taylor & Francis Group

Horizontal advection of temperature and salinity by Rossby waves in the North Pacific

Tatyana V. Belonenko[a], Igor L. Bashmachnikov[a,b] and Arseny A. Kubryakov[c]

[a]St. Petersburg State University, Saint Petersburg, Russia; [b]NIERSC- Nansen International Environmental and Remote Sensing Centre, Saint Petersburg, Russia; [c]Remote Sensing Department, The Marine Hydrophysical Institute, Sevastopol, Russia

ABSTRACT

The Aquarius satellite has been used for the first time to characterize Rossby waves in sea surface salinity (SSS) measurements for the North Pacific Ocean. Westward propagating wave signals are delineated by the SSS zonal salinity gradients. The phase velocities and spectral properties obtained from zonal salinity gradients are closely correlated with corresponding values obtained from the sea surface temperature (SST) zonal gradient and the altimetry-derived meridional velocity. The westward propagating SSS signals are consistent with Rossby wave advection across the strong meridional gradients of water characteristics. Following Killworth, we attempted to provide satellite-based estimates of the contribution of horizontal Rossby wave advection to the surface transfer of temperature and salinity in the North Pacific Ocean. Westward propagating signals in the SST and SSS zonal gradient fields show that the observed intensity of meridional advection by the ambient gradients of SST and SSS is less than the intensity predicted by an analytical solution of the transfer equation for Rossby waves. Our results extend the previous studies of physical mechanisms of Rossby wave manifestation at the sea surface and we demonstrate that Rossby waves are responsible for low-frequency oscillations in SST and SSS concentration in the North Pacific.

ARTICLE HISTORY
Received 8 April 2017
Accepted 14 December 2017

1. Introduction

The Rossby waves in the open ocean are westward propagating disturbances which owe their existence to the rotation and sphericity of the Earth. They convey information westwards, linking processes in the west of ocean basins with other processes that occurred earlier in the east (see a review by Colin de Verdiere and Tailleux 2005). Baroclinic Rossby waves are clearly seen from satellite altimetry as the westward propagating signals in time-longitude diagrams of sea level. The signal propagation velocities are close to the phase speed of long linear baroclinic Rossby waves of the first vertical

CONTACT Tatyana V. Belonenko btvlisab@yandex.ru Saint Petersburg State University, 10th line 33/35, St. Petersburg, 199178, Russia

- Rossby waves are observed in Aquarius sea surface salinity (SSS) measurements in the North Pacific.
- Spectral properties of SSS agree with characteristics of meridional velocity disturbances.
- Theory of Rossby waves advection overestimates variability of SSS and sea surface temperature (SST).
- Transport mechanism of the wave signatures in SST with Rossby waves works the same way as in SSS.

mode with the corresponding wavelength (Colin de Verdiere and Tailleux 2005). This serves the principal argument for interpretation of westward propagation of the observed disturbances as Rossby waves (Chelton and Schlax 1996; Killworth, Chelton, and de Szoeke 1997; Belonenko 2012a; 2012b). Similar signals are observed in satellite SST and chlorophyll-a measurements, affecting distributions of ocean thermohaline properties and ecosystems (Cipollini et al. 1997; 2001; Cipollini 2003; Quartly et al. 2003; Killworth et al. 2004; Charria et al. 2008; Belonenko, Koldunov, and Foux 2011). These anomalies are thought to be induced by horizontal or vertical advection in Rossby waves and/or by surface/subsurface mesoscale eddies (Quartly et al. 2003; Killworth et al. 2004; Charria et al. 2008; Chelton et al. 2011a; Chelton, Schlax, and Samelson 2011b; Bashmachnikov, Belonenko, and Koldunov 2013a; 2013b; 2014). A linear theory of this mechanism has been proposed and tested for SST and chlorophyll-a data (Killworth et al. 2004).

Aquarius satellite sea surface salinity (SSS) measurements, available since 2011, allow detection of tropical instability waves (Lee et al. 2012) and annual-period planetary wave (Menezes, Vianna, and Phillips 2014). The effect of Rossby waves on SSS data was studied for the tropical Indian Ocean with using the HYCOM (Hybrid Coordinate Ocean Model) numerical model (Heffner, Subrahmanyam, and Shriver 2008). In this research we document the Rossby waves observed in the Aquarius SSS measurements in the tropical, the subtropical and the mid-latitudes of the North Pacific (15°–50° N) and investigate the effect of horizontal advection by Rossby waves on the observed SSS disturbances.

2. Data and methods

2.1. *Sea surface salinity (SSS)*

In the present study we use SSS measurements received from the Aquarius/SAC-D satellite, which is a collaborative effort between NASA and the Argentinean Space Agency (Comision Nacional de Actividades Espaciales – CONAE). Weekly maps of the Aquarius SSS fields Level 3, V2.0, from August 2011 to January 2015 and with the spatial resolution of 1°×1°, are obtained from the PODAAC (Physical Oceanography Distributed Active Archive Center, http://podaac.jpl.nasa.gov/). After the release of initial version of Aquarius SSS data, significant updates for the salinity retrieval algorithm have been made many times, which improves some bias problem found in early version of Aquarius product (Lagerloef et al. 2015). However, the Aquarius SSS fields Level 3, V2.0 allow identifying the effect of horizontal advection by Rossby waves in the variability of Aquarius SSS data. See also Kubryakov et al. (2016).

2.2. *Sea surface temperature (SST)*

We use the Reynolds NOAA (National Oceanic and Atmospheric Administration) Optimum Interpolation Sea Surface Temperature (SST) data (Reynolds and Smith 1994; Reynolds et al. 2007) for 2011–2015 based on the merged measurements of the Advanced Very High Resolution Radiometer (AVHRR) and the Advanced Microwave Scanning Radiometer (AMSR) combined with ship and buoy observations [http://www.

ncdc.noaa.gov/sst/]. The data has a spatial grid resolution of 0.25° and temporal resolution of 1 day.

2.3. *Satellite altimetry*

In this work we use AVISO absolute dynamic topography (ADT) and geostrophic velocities for 2011–2015 constructed from multi-mission merged sea level anomaly (SLA) and Mean Dynamic Topography (Rio, Guinehut, and Larnicol 2011). The AVISO altimetry products are produced by Ssalto/Duacs (Le Traon, Nadal, and Ducet 1998) and distributed by AVISO, with support from CNES (Centre National d'Etudes Spatiales) [http://www.aviso.altimetry.fr/duacs/]. The spatial resolution of the weekly gridded data is 0.25° × 0.25°. From the sea-level data, the meridional component of the geostrophic current velocity (v) is computed as the zonal gradient of ADT: $v = \frac{g}{f}\ \frac{\partial h}{\partial x}$, h means ADT. Here, f is the Coriolis parameter and g is the gravitational acceleration.

3. Rossby waves observed in SSS measurements

In the open ocean the climatic isolines of SSS are mostly zonal and the mean zonal gradients are small as compared to the meridional ones. Therefore, the meridional water advection, induced by waves or eddies is the most pronounced in the zonal gradients of ocean properties (Chelton and Schlax 1996). Zonal SSS gradients (S_x and the subscript x means $\frac{\partial}{\partial x}$ here and onwards) are analyzed for three latitudes located in the northern hemisphere. Regular errors of SSS data are excluded in S_x. On time-longitude diagrams of the Aquarius-derived SSS zonal gradients (S_x), westward propagation signals are clearly seen (Figure 1(a, d, g)). For comparison, the diagrams of SST zonal gradients (T_x), (are also presented (Figure 1(b, e, h)). To reduce noise, in Figure 1 the S_x and T_x longitude-time diagrams are smoothed using the running average with the window size of 2 weeks and of 1° degree in longitude. Time-longitude diagrams for altimetry data for the same region and time range are presented in (Belonenko, Kubrjakov, and Stanichny 2016). The spatial scales of S_x and T_x in the time-longitude diagrams and their tilt to 'x'-axis (the propagation velocity) agree with each other as well as with v (Figure 1(c, f, i)), and show similar variation with latitude (Figure 1).

The characteristic velocity (c) of the westward propagating signals in T_x and S_x, as well as in meridional geostrophic velocity v, are estimated using the Radon transform (Challenor, Cipollini, and Cromwell 2001) with a specific longitude – time running window for each latitude (Belonenko and Kubrjakov 2014). The theoretical phase velocity of the westward propagating signals in SLA are displayed in Belonenko, Kubrjakov, and Stanichny (2016), where the authors compare it using the baroclinic Rossby deformation radius in the WKB-approximation (named after Wentzel, Kramers, and Brillouin) and determined by the two-layer fluid model with latitude-mean phase velocity calculated from altimetry data by the Radon transform. In order to obtain the spatio-temporal variability of $c(v)$, $c\,(T_x)$ and $c\,(S_x)$, the Radon transform is applied using Figure 2(a and b), which shows that there exists a significant variability of $c\,(T_x)$ and $c\,(S_x)$. Velocity of the propagating disturbances increases to the south-west, in agreement with the increase of the first baroclinic Rossby radius of deformation (Chelton et al. 1998). The transition area between the low and the high velocity values (35° N, 150° E – 20° N,

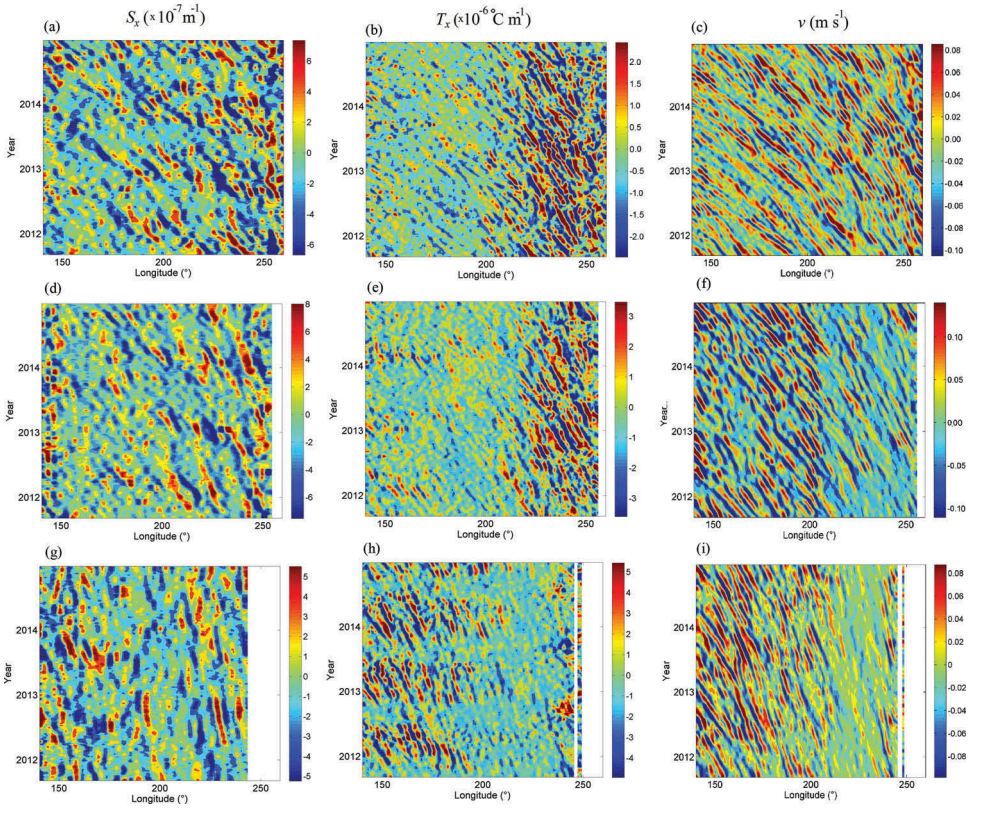

Figure 1. Time-longitude plots of: zonal SSS gradients S_x at 16° N (a), 19° N (d) and 28° N (g); zonal SST gradients T_x at 16° N (b), 19° N (e) and 28° N (h); $v = \frac{g}{f}\frac{\partial h}{\partial x}$ at 16° N (*c*), 19° N (f) and 28° N (i).

250° E) matches with the position of the subtropical frontal zone, which separates the light upper ocean water of the central subtropical gyre from the denser waters of its northeastern periphery.

The mean meridional variations of velocity computed from time-longitude diagrams of v, T_x and S_x are shown in Figure 2(c). Red line shows the speed of westward propagating signals of the meridional current velocity component, $c(v)$, computed using altimetry data. The three independent estimates have similar meridional variations, decreasing from about 0.07–0.11 m s^{-1} at 15° N to around 0.01 m s^{-1} at 60° N. The difference between the propagation velocities, based on altimetry ($c(v)$) and SST data ($c(T_x)$), estimated as the standard deviation of the differences between the c values at the same latitudes, is only around 0.004 m s^{-1}. In comparison to $c\,(T_x)$ and $c\,(v)$, the SSS-based estimates are biased to lower values at 20°–25° N and higher values at 30°–50° N. We attribute those discrepancies to a stronger spatial smoothing of the results, computed from SSS data. Precipitation, as well as local variations of the heat flux across the sea surface, can also influence the local variance of SSS and SST, increasing noise level of these datasets, as compared to altimetry. However, Belonenko, Kubrjakov, and Stanichny (2016) demonstrated that the characteristic empirical propagation velocities, obtained using the Radon transform, closely correspond to

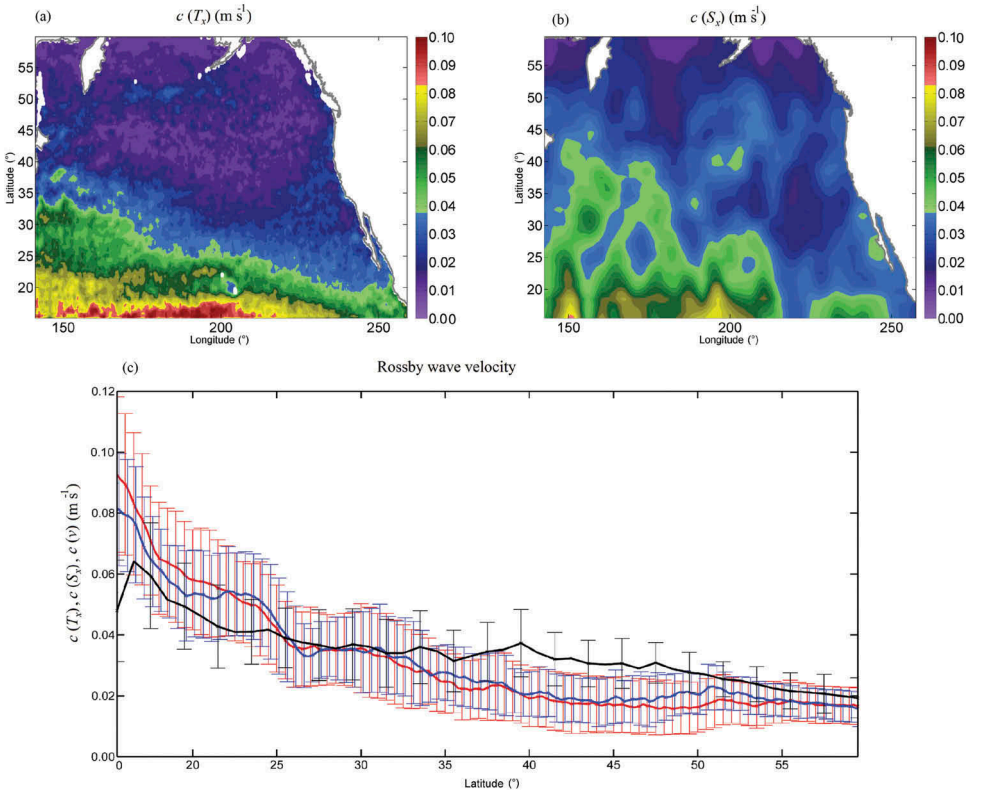

Figure 2. Time-averaged map of the absolute value of the Rossby wave velocity c, computed from T_x (a) and S_x (b). Latitudinal variability of the absolute value of the Rossby wave velocity, computed from T_x (blue) and S_x (green) and $c(v)$ (red); the vertical colour bars shown at each latitude are 95% confidence interval. All presented velocities are westwards.

the theoretical phase velocity of long linear Rossby waves of the first vertical mode for the corresponding latitudes. The typical periods of the most energetic oscillations are from 1 to 3 months. Figure 3 provides a good agreement between empirical and theoretical phase velocity of the Rossby waves.

Figure 3 presents the spectral densities of $c\,(v)$, $c\,(T_x)$ and $c\,(S_x)$ computed using the 2D fast Fourier transform. Before the analysis, the mean seasonal variations were subtracted from data. The spectral densities, derived from the three datasets have similar distributions in (σ, k)-space. Black straight lines in Figure 3 present the phase velocity of the propagating disturbances, calculated from altimetry data using Radon transform. The phase velocity estimates obtained corresponds well to the theoretical phase velocity of propagating long linear baroclinic Rossby waves (Killworth, Chelton, and de Szoeke 1997; Killworth and Blundell 2003a; 2003b). Following previous studies, we relate the observed westward propagation of the anomalies to a meridional advection of the predominantly zonally distributed mean climatic state by westward going Rossby waves or by swirl velocities of mesoscale eddies (Quartly et al. 2003; Killworth et al. 2004; Charria et al. 2008; Chelton, Schlax, and Samelson 2011b).

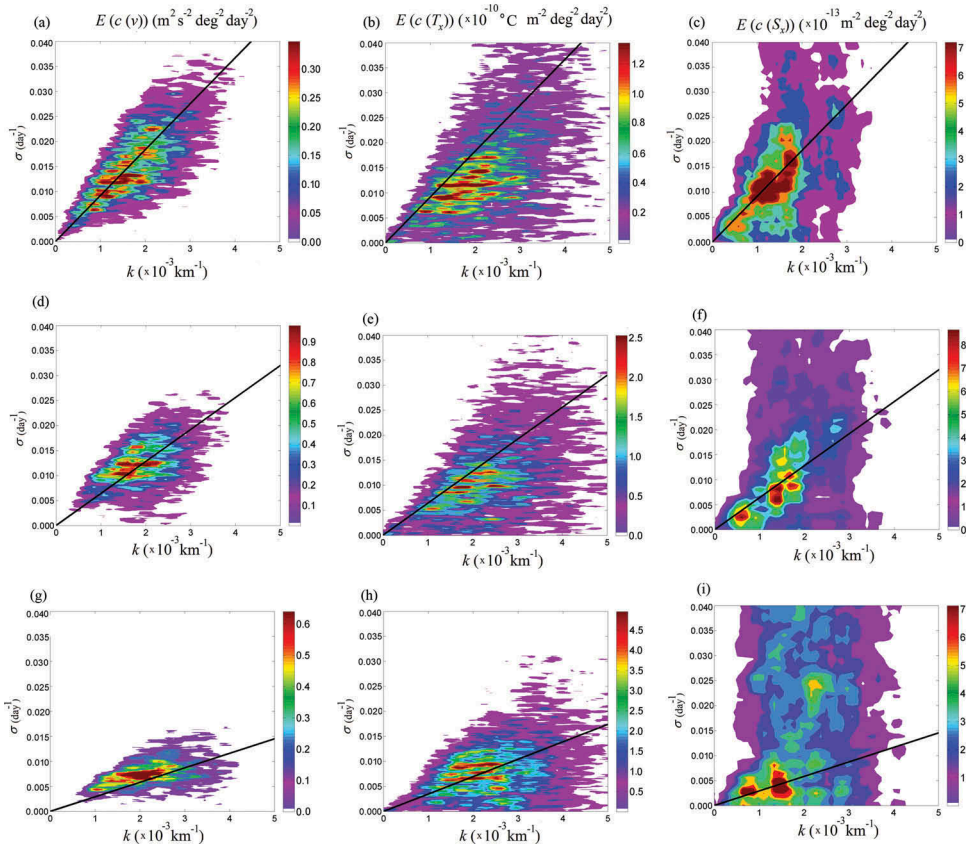

Figure 3. Distribution of spectral energy density E in (σ, k) space: at 15.5° N $c(v)$ (a), c (T_x) (b), c (S_x) (c); at 18.5° N $c(v)$ (d), c (T_x) (e), c (S_x) (f); at 28.5° N $c(v)$ (g), c (T_x) (h), c (S_x) (i). The black line shows the mean phase velocity computed from altimetry data. The ordinate is the frequency σ (day^{-1}). Black lines are theoretical phase velocity of long linear Rossby waves.

Figure 3 also shows a significant increase of the noise in the S_x spectrum towards higher latitudes. The spatial scales of waves and eddies are smaller at higher latitudes (Chelton, Schlax, and Samelson 2011b), and it seems that the current spatial resolution of Aquarius SSS (1°×1°) is insufficient to capture the observed variations of smaller wavelength in the northern part of the study region, leading to the signal aliasing. Furthermore, accuracy of the SSS derivation algorithm decreases with a decreasing temperature. This adds noise to the SSS data at high latitudes in the northern Hemisphere (Lagerloef et al. 2010; Lagerloef et al. 2015; Kao and Lagerloef 2015).

4. Horizontal advection of SSS and SST by linear Rossby waves

In this section we compare the analytical solution for horizontal advection of a passive tracer (which may be water particles with the conserved SST and SSS) by Rossby waves

with observations. The analytic solution is similar to the one obtained by Killworth et al. (2004) with some modifications.

We consider the transport equation of heat/salt balance, where we neglect forcing and the vertical component of the current velocity (LeBlond and Mysak, 1978):

$$\frac{\partial G}{\partial t} + u\frac{\partial G}{\partial x} + v\frac{\partial G}{\partial y} = 0 \tag{1}$$

Here G is either SSS or SST, u and v are the eastward and northward current velocities, respectively. We further decompose the signal into the mean background state $(\bar{u}, \bar{v}, \bar{G})$ and the wave perturbations (u', v', G'). Assuming that (1) also holds for the mean parameter distribution and neglecting the products of perturbations, as compared to the products of perturbations and the mean fields, the equation is reduced to

$$\frac{\partial G'}{\partial t} + \bar{u}\frac{\partial G'}{\partial x} + u'\frac{\partial \bar{G}}{\partial x} + \bar{v}\frac{\partial G'}{\partial y} + v'\frac{\partial \bar{G}}{\partial y} = 0 \tag{2}$$

In the open ocean, mean currents are mostly zonal, and we set $\bar{v} = 0$. Also, we assume that the SST/SSS fields predominantly change in the meridional direction, and the mean zonal gradients of SST/SSS are significantly less than the meridional ones. Therefore, $u'\frac{\partial \bar{G}}{\partial x} << v'\frac{\partial \bar{G}}{\partial y}$. For the periodically oscillating disturbances, we write $v'(t,x,y) = A(y)\, e^{i(\sigma t - kx)}$, where $A(y)$ is the wave amplitude, $\sigma > 0$ is the wave frequency and k is the zonal wavenumber. Equation (2) becomes:

$$\frac{\partial G'}{\partial t} + \bar{u}\frac{\partial G'}{\partial x} = -A(y)\, e^{i(\sigma t - kx)}\frac{\partial \bar{G}}{\partial y}. \tag{3}$$

For a constant mean zonal flow $\bar{u}$ the full solution of equation (3) is (Polyanin and Zaitsev 2012):

$$G'(t,\ x,y) = \begin{cases} \frac{-A(y)\frac{\partial \bar{G}}{\partial y}}{i(\sigma - \bar{u}k)} e^{i(\sigma t - kx)} + \Phi(\bar{u}\, t - x), & \sigma - \bar{u}\, k \neq 0, \\ -A(y)\frac{\partial \bar{G}}{\partial y}\ t\, e^{i(\sigma t - kx)} + \Phi(\bar{u}\, t - x), & \sigma - \bar{u}\, k = 0 \end{cases} \tag{4}$$

Here Φ is a self-similar solution of equation (3). For $t = 0, \quad x = 0$, the function $\Phi(0) = G(0,\ 0, y) = G_0(y)$ describes an initial mean meridional profile of the function G. Expression (4) shows that the dominating frequencies, wavenumbers and phase velocities of the disturbances of $G'(t,\ x, y)$ agree with the corresponding spectral characteristics of the meridional component of the current velocity v' which characterizes the Rossby waves (see also Belonenko, Koldunov, and Foux 2011; Belonenko, 2012b). The lower line in expression (4) presents a particular case of the resonant wave-current interaction, when the mean zonal current velocity $(\bar{u})$ is close to the phase speed of a Rossby wave $(c = \sigma/k)$. The predicted linear growth of the amplitude will certainly take place only at the initial stages of the resonant interaction, as further on the non-linear terms, neglected in equation (2), will limit the growth. The first term in expression (4) is a particular solution, which shows that temperature/salinity perturbations are related to the amplitude of the meridional velocity of the oscillations as well as to the background meridional gradients of the SST/SSS fields. To obtain spectral evaluation, we get after differentiating expression (4) in x and neglecting Φ:

$$\frac{\partial G'}{\partial x} = \frac{A(y)\frac{\partial \bar{G}}{\partial y}}{(c-\bar{u})} e^{i(\sigma t - kx)}.$$

Then the squared amplitude is:

$$\left(\frac{\partial G'}{\partial x}\right)^2 = A(y)^2 \left(\frac{\partial \bar{G}}{\partial y}\right)^2 / (c-\bar{u})^2 \tag{5}$$

The left-hand side of expression (5) is proportional to the spectral energy density of T_x or S_x at a selected (σ, k), as the one obtained from observations (Figure 3).

The right-hand side, $F(G) = A(y)^2 \left(\frac{\partial \bar{G}}{\partial y}\right)^2 / (c-\bar{u})^2$, provides an impact of meridional velocity v', induced by a Rossby wave, on mean state of the variable G with the mean zonal gradient $\frac{\partial \bar{G}}{\partial y}$.

Figure 4 presents latitudinal variability of spectral energy density of T_x and S_x zonally averaged from 160° to 200° of longitude, estimated from satellite data in the North Pacific (the black lines). For estimating the right-hand side of Equation (5), the zonal velocity of the background flow $\bar{u}$ is obtained from the period 2011–2015 mean zonal velocities, derived from AVISO altimetry, $\frac{\partial \bar{G}}{\partial y}$ is computed as the mean meridional gradient of T_x and S_x. $A(y)^2$ is the peak value of spectral energy density of the zonal gradient of ADT ($v = \frac{g}{f}\frac{\partial h}{\partial x}$, see distributions in (σ, k) in Figure 3(a, d, g)), averaged over the selected longitude range at each latitude. In these limits the assumptions of the predominantly zonal mean flow and the meridional direction of the mean gradients of SST/SSS hold relatively well. For T_x, spectral energy densities, derived from observations, $\left(\frac{\partial G'}{\partial x}\right)^2$, as well as their theoretical estimates $(A(y))^2 \left(\frac{\partial \bar{G}}{\partial y}\right)^2 / (c-\bar{u})^2$, both increase towards the subpolar frontal zone at 35°–45° N, where the meridional SST gradients are the largest. For S_x, two maxima of $(A(y))^2 \left(\frac{\partial \bar{G}}{\partial y}\right)^2 / (c-\bar{u})^2$ are observed in the areas of the subtropical front (30°–35° N) and of

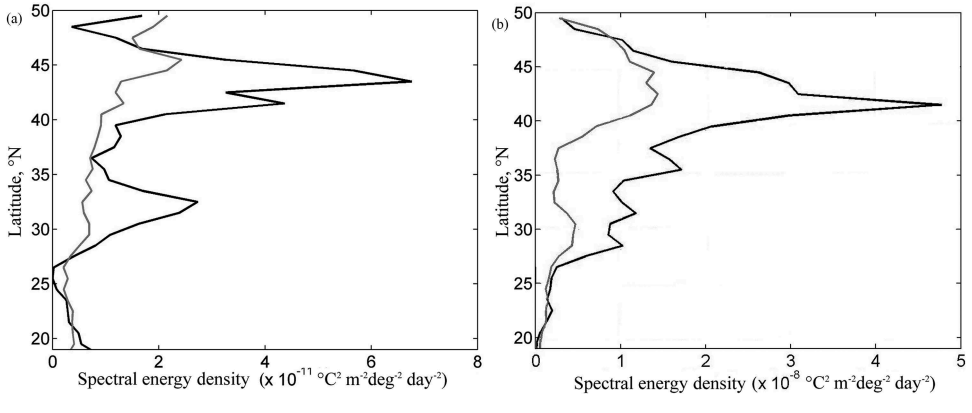

Figure 4. Latitudinal variability of spectral energy density $\left(\frac{\partial G'}{\partial x}\right)^2$ averaged over 160°–200° of longitude over the whole frequency-wave number domain for (a) $\frac{\partial G'}{\partial x} = T_x$ (°C m^{-1}); (b) $\frac{\partial G'}{\partial x} = S_x$ (m^{-1}); grey lines show $\left(\frac{\partial G'}{\partial x}\right)^2$, black lines indicate $A(y)^2 \left(\frac{\partial \bar{G}}{\partial y}\right)^2 / (c-\bar{u})^2$.

the subpolar front (40°–45° N). The spectral energy densities of S_x, $\left(\frac{\partial G'}{\partial x}\right)^2$, show a pronounced peak only in the area of the subpolar front, although the subtropical front is marked with a certain increase between 25° N and 30° N as well.

However, around their maxima, the spectral energy densities of T_x and S_x, derived from satellite data, are 2–4 times less than those, expected as a result of the advection by long linear Rossby waves predicted by expression (5). The results agree with those by Killworth et al. (2004), who showed that the amplitudes of the meridional advection of chlorophyll-a observed are 1–3 times less than those predicted by the theory of long linear Rossby waves. The reason for the discrepancies can be related to a non-conservative behavior of SST, SSS and chlorophyll-a fields in the real ocean. It can be also attributed to the effects of horizontal and vertical turbulent diffusion or of other nonlinear terms, neglected in expression (5). Finally, non-linear character of Rossby waves or the dominance of mesoscale eddies (Chelton, Schlax, and Samelson 2011b) would result in less efficient meridional transport of the tracers, as compared to that, predicted by the linear theory of Rossby waves.

5. Conclusions

The Aquarius satellite salinity measurements give a possibility to observe an impact of Rossby waves on the ocean surface salinity, as the corresponding SSS zonal gradients significantly exceed the zonal gradients of the mostly zonally aligned climatic salinity fields. Our analysis shows that the SSS zonal gradients in the North Pacific are forming wave-like structures in Hovmoller diagrams, similar to those in the SST zonal gradients or altimetry derived meridional current velocities. The spectral density maxima of westward S_x in (σ, k)-space are found to follow the dispersion relation for linear baroclinic Rossby waves of the first vertical mode. The dominating frequencies, wavenumbers and phase velocities of the SSS disturbances essentially agree with the corresponding spectral characteristics of the SST disturbances, as well as with those of the meridional current velocity. This seems to indicate that the anomalies are formed via meridional advection of water properties by long Rossby waves.

The linear theory of Rossby waves allows a quantitative estimate of the intensity of the meridional advection, and is further compared with the spectral density of the zonal gradients of SST and of SSS. The expected meridional advection intensity by linear Rossby waves is found to be 2–4 times higher than the observed one for both tracers at 35°–45° N. Sharp peaks show up at 28°, 36.5°, 41.4° and 43.5° N for SST, and 32°, 41.4° and 43.5° N for SSS. Previously, similar results were obtained by Killworth et al. (2004) for chlorophyll-a data. In the zonally averaged values of the predicted and modelled spectral densities of S_x and T_x, the highest differences are detected in the areas of strong eastwards mean zonal currents. Non-linear behavior of Rossby waves or enhanced horizontal diffusion in the regions of the strong horizontal mean current shear may be the reasons for the observed discrepancies.

Acknowledgments

The AVISO altimetry products are produced by Ssalto/Duacs and distributed by AVISO, with support from CNES [http://www.aviso.altimetry.fr/duacs/]. SSS data were obtained freely from

Physical Oceanography Distributed Active Archive Center (ftp://podaac-ftp.jpl.nasa.gov/allData/aquarius/L3/mapped/V3/). The research was supported by Russian Foundation for Basic Research (projects no. 16-05-00452 and no. 17-05-00034). Kubryakov A.A. was supported by the Russian Science Foundation, the research grant 15-17-20020.

Disclosure statement

No potential conflict of interest was reported by the authors.

Funding

This work was supported by Russian Foundation for Basic Research [17-05-00034]; Russian Foundation for Basic Research [16-05-00452, 17-05-00034]; Russian Science Foundation [15-17-20020];

References

Bashmachnikov, I., T. V. Belonenko, and A. V. Koldunov. 2013a. "Intra-Annual and Interannual Non-Stationary Cycles of Chlorophyll Concentration in the North-East Atlantic." *Remote Sensing of Environment* 137: 55–68. doi:10.1016/j.rse.2013.05.025.

Bashmachnikov, I., D. Boutov, and J. Dias. 2013b. "Manifestation of Two Meddies in Altimetry and Sea-Surface Temperature." *Ocean Science* 9: 249–259. doi:10.5194/os-9-249-2013.

Bashmachnikov, I., X. Carton, and T. Belonenko. 2014. "Characteristics of Surface Signatures of Mediterranean Water Eddies." *Journal of Geophysical Research* C119. doi:10.1002/2014JC010244.

Belonenko, T. V. 2012a. "Rossby Waves Observation in the Northwestern Pacific." *Sovremennye Problemy Distantsionnogo Zondirovaniya Zemli Iz Kosmosa* 9 (3): 209–215. (in Russian).

Belonenko, T. V. 2012b. "The Relationship between Low-Frequency Variability of the Heat Advection and of the Sea Level in the NW Pacific Ocean." *Sovremennye Problemy Distantsionnogo Zondirovaniya Zemli Iz Kosmosa* 9 (5): 260–269. (in Russian).

Belonenko, T. V., A. V. Koldunov, and V. R. Foux. 2011. "Advecting Chlorophyll by Rossby Waves." *Vestnik Saint-Petersburgskogo Universiteta Series* 7 (4): 106–109. (In Russian).

Belonenko, T. V., and A. A. Kubrjakov. 2014. "Temporal Variability of the Phase Velocity of Rossby Waves in the North Pacific." *Sovremennye Problemy Distantsionnogo Zondirovaniya Zemli Iz Kosmosa* 11 (3): 9–18. (in Russian).

Belonenko, T. V., A. A. Kubrjakov, and S. V. Stanichny. 2016. "Spectral Characteristics of Rossby Waves in the Northwestern Pacific Based on Satellite Altimetry Izvestiya." *Atmospheric and Oceanic Physics* 52 (9): 920–928. doi:10.1134/S0001433816090073.

Challenor, P. G., P. Cipollini, and D. Cromwell. 2001. "Use of the 3D Radon Transform to Examine the Properties of Oceanic Rossby Waves." *Journal Atmos Oceanic Technological* 18: 1558–1566. doi:10.1175/1520-0426(2001)018<1558:UOTRTT>2.0.CO;2.

Charria, G., I. Dadou, P. Cipollini, M. Drévillon, and V. Garçon. 2008. "Influence of Rossby Waves on Primary Production from a Coupled Physical–Biogeochemical Model in the North Atlantic Ocean." *Ocean Science* 4: 199–213. doi:10.5194/os-4-199-2008.

Chelton, D., and M. Schlax. 1996. "Global Observations of Oceanic Rossby Waves." *Science* 272 (5259): 234–238. doi:10.1126/science.272.5259.234.

Chelton, D. B., R. A. Deszoeke, M. G. Schlax, K. El Naggar, and N. Siwertz. 1998. "Geographical Variability of the First Baroclinic Rossby Radius of Deformation." *Journal of Physical Oceanography* 28 (3): 433–460. doi:10.1175/1520-0485(1998)028<0433:GVOTFB>2.0.CO;2.

Chelton, D. B., P. Gaube, M. G. Schlax, J. J. Early, and R. M. Samelson. 2011a. "The Influence of Nonlinear Mesoscale Eddies on Near-Surface Oceanic Chlorophyll." *Science* 334 (6054): 328–332. doi:10.1126/science.1208897.

Chelton, D. B., M. G. Schlax, and R. N. Samelson. 2011b. "Global Observations of Nonlinear Mesoscale Eddies." *Progress in Oceanography* 91: 167–216. doi:10.1016/j.pocean.2011.01.002.

Cipollini, P. 2003. "Multiple Satellite Observations of Oceanic Planetary Waves: Techniques and Findings." In *Proceedings of 2003 Tyrrhenian International Workshop on Remote Sensing*, Ed. E. D. Mese, 134–143. Italy: Edizioni Plus, University of Pisa.

Cipollini, P., D. Cromwell, P. G. Challenor, and S. Raffaglio. 2001. "Rossby Waves Detected in Global Ocean Colour Data." *Geophys Researcher Letters* 28 (2): 323–326. doi:10.1029/1999GL011231.

Cipollini, P., D. Cromwell, M. S. Jones, G. D. Quartly, and P. G. Challenor. 1997. "Concurrent Altimeter and Infrared Observations of Rossby Wave Propagation near 34°N in the Northeast Atlantic." *Geophys Researcher Letters* 24: 889–892. doi:10.1029/97GL00758.

Colin de Verdiere, A., and R. Tailleux. 2005. "The Interaction of a Baroclinic Mean Flow with Long Rossby Waves." *Journal of Physical Oceanography* 35: 865–879. doi:10.1175/JPO2712.1.

Heffner, D. M., B. Subrahmanyam, and J. F. Shriver. 2008. "Indian Ocean Rossby Waves Detected in HYCOM Sea Surface Salinity." *Geophysical Research Letters* 35: L03605. doi:10.1029/2007GL032760.

Kao, H.-Y., and G. S. E. Lagerloef. 2015. "Salinity Fronts in the Tropical Pacific Ocean." *Journal Geophys Researcher Oceans* 120: 1096–1106. doi:10.1002/2014JC010114.

Killworth, P., D. Chelton, and R. de Szoeke. 1997. "The Speed of Observed and Theoretical Long Extratropical Planetary Waves." *Journal of Physical Oceanography* 27 (9): 1946–1966. doi:10.1175/1520-0485(1997)027<1946:TSOOAT>2.0.CO;2.

Killworth, P. D., and J. R. Blundell. 2003a. "Long Extra-Tropical Planetary Wave Propagation in the Presence of Slowly Varying Mean Flow and Bottom Topography: I. The Local Problem." *Journal of Physical Oceanography* 33: 784–801. doi:10.1175/1520-0485(2003)33<784:LEPWPI>2.0.CO;2.

Killworth, P. D., and J. R. Blundell. 2003b. "Long Extra-Tropical Planetary Wave Propagation in the Presence of Slowly Varying Mean Flow and Bottom Topography: II. Ray Propagation and Comparison with Observations." *Journal of Physical Oceanography* 33: 802–821. doi:10.1175/1520-0485(2003)33<802:LEPWPI>2.0.CO;2.

Killworth, P. D., P. Cipollini, U. B. Mete, and J. R. Blundell. 2004. "Physical and Biological Mechanisms for Planetary Waves Observed in Satellite-Derived Chlorophyll." *Journal of Geophysical Research* 109 (C7): C07002-[18pp]. doi:10.1029/2003JC001768.

Kubryakov, A., S. Stanichny, and A. Zatsepin. 2016. "River Plume Dynamics in the Kara Sea from Altimetry-Based Lagrangian Model, Satellite Salinity and Chlorophyll Data." *Remote Sensing of Environment* 176: 177–187. doi:10.1016/j.rse.2016.01.020.

Lagerloef, G., J. Boutin, Y. Chao, T. Delcroix, J. Font, P. Niiler, and F. Wentz. 2010. "Resolving the Global Surface Salinity Field and Variations by Blending Satellite and in Situ Observations." *Proceedings of Ocean Obs* 9: 21–25.

Lagerloef, G., H.-Y. Kao, T. Meissner, and J. Vazquez. 2015. *Aquarius Salinity Validation Analysis; Data Version 4.0, Aquarius Project Document: AQ-014-PS-0016*, 30. ftp://podaac-ftp.jpl.nasa.gov/allData/aquarius/docs/v4/AQ-010-UG-0008_AquariusUserGuide_DatasetV4.0.pdf

Le Traon, P.-Y., F. Nadal, and N. Ducet. 1998. "An Improved Mapping Method of Multisatellite Altimeter Data." *Journal Atmos Oceanic Technological* 15: 522–534. doi:10.1175/1520-0426(1998)015<0522:AIMMOM>2.0.CO;2.

LeBlond, P. H., and L. A. Mysak. 1978. *Waves in the Ocean*, 602 p. Amsterdam: Elsevier.

Lee, T., G. Lagerloef, M. M. Gierach, H.-Y. Kao, S. Yueh, and K. Dohan. 2012. "Aquarius Reveals Salinity Structure of Tropical Instability Waves." *Geophys Researcher Letters* 39: L12610. doi:10.1029/2012GL052232.

Menezes, V. V., M. L. Vianna, and H. E. Phillips. 2014. "Aquarius Sea Surface Salinity in the South Indian Ocean: Revealing Annual-Period Planetary Waves." *Journal Geophys Researcher Oceans* 119: 3883–3908. doi:10.1002/2014JC009935.

Polyanin, A. D., and V. F. Zaitsev. 2012. *Handbook of Nonlinear Partial Differential Equations*. Boca Raton–London: Chapman and Hall/CRC Press.

Quartly, G. D., P. Cipollini, D. Cromwell, and P. G. Challenor. 2003. "Rossby Waves: Synergy in Action." *Philosophical Transactions. Series A, Mathematical, Physical, and Engineering Sciences* 361 (1802): 57–63. doi:10.1098/rsta.2002.1108.

Reynolds, R. W., and T. M. Smith. 1994. "Improved Global Sea Surface Temperature Analyses Using Optimum Interpolation." *Journal of Climate* 7: 929–948. doi:10.1175/1520-0442(1994)007<0929:IGSSTA>2.0.CO;2.

Reynolds, R. W., T. M. Smith, C. Liu, D. B. Chelton, K. S. Casey, and M. G. Schlax. 2007. "Daily High-Resolution Blended Analyses for Sea Surface Temperature." *Journal of Climate* 20: 5473–5496. doi:10.1175/2007JCLI1824.1.

Rio, M. H., S. Guinehut, and G. Larnicol. 2011. "New CNES-CLS09 Global Mean Dynamic Topography Computed from the Combination of GRACE Data, Altimetry, and in Situ Measurements." *Journal of Geophysical Research* 116: C07018. doi:10.1029/2010JC006505.